



Conformational properties of hybrid star-shaped polymers comprised of linear and ring arms

Khristine Haydukivska,^{1,2} Viktoria Blavatska ,¹ Jarosław S. Kłos,^{3,4} and Jarosław Paturej ^{2,4,*}

¹*Institute for Condensed Matter Physics of the National Academy of Sciences of Ukraine, 79011 Lviv, Ukraine*

²*Institute of Physics, University of Silesia, 41-500 Chorzów, Poland*

³*Faculty of Physics, A. Mickiewicz University, Uniwersytetu Poznańskiego 2, 61-614 Poznań, Poland*

⁴*Leibniz-Institut für Polymerforschung Dresden e.V., 01069 Dresden, Germany*



(Received 3 December 2021; accepted 4 February 2022; published 8 March 2022)

We study the influence of arm architecture on the conformational properties of hybrid star-shaped macromolecules called rosette polymers containing linear and ring grafts connected to a central branching point in a good solvent regime. We utilize analytical methods and molecular dynamics simulations to determine the estimates for the relative size ratios of these polymers with respect to linear chains and starlike polymers composed of the same number of solely linear arms and equal molecular weights. The results of numerical simulations corroborate our theoretical prediction that rosette polymers undergo conformational compactification with increasing functionality of grafted rings. Our results quantitatively describe the impact of the complex architecture of the molecules with excluded volume on their effective size measures.

DOI: [10.1103/PhysRevE.105.034502](https://doi.org/10.1103/PhysRevE.105.034502)

I. INTRODUCTION

Polymers with complex macromolecular architectures are in focus of current polymer science due to their unique physical properties. One of the examples of branched polymer topology is a starlike macromolecule containing a number of linear chains grafted with one end to the central core. Star polymers are considered hybrids between polymer entities and colloids [1]: by increasing the number of grafted arms, f_L , their conformations continuously transform from soft polymer coils ($f_L = 1, 2$) to rigid, colloidal spheres ($f_L \gg 1$). As a result, star polymers reveal a number of features which do not occur in solutions of linear chains and in suspensions of colloids. Star polymers are characterized by a compact structure and an enhanced segmental density [2–10] as compared to linear polymers of the same molecular weight. Star-shaped polymers modify surface tension [11], glass temperature [12], surface wettability [13], possess hierarchical dynamics [14,15], and complex rheological properties [16,17]. Star polymers are also important from an application point of view [18]. For instance, they are used in the oil industry as lubricants [19], binders in toners for copying machines [20], and in numerous medical applications [21] as vectors to deliver peptides [22] or drugs [23]. Besides linear polymers other molecular architectures can be utilized to construct star-shaped macromolecules. The distinct example is cyclic polymers which have no free ends. This kind of molecular topology of nongrafted rings enforces their markedly different properties in solutions as compared to linear counterparts, including smaller radius of gyration, smaller hydrodynamic volume, lower melt viscosity, and higher thermostability [2,6,24–31]. The compactness of cyclic polymers

determines unique mechanical properties such as lack of plateau modulus in melts [31], much larger swelling ability, and maximum strain at break for swollen networks [32]. The cyclic architecture of polymers is also the major factor triggering frictional forces of polymer-grafted surfaces under shear [33,34]. Ring polymers can be found in living cells in bacteria [35] and in higher eucaryotes [36] which contain the circular DNA. Structures with rings are also encountered in nature during the process of loop formation that plays an important role in stabilization of globular proteins [37–40], DNA compactification in the nucleus [41–43], and gene regulations [44–46]. Incorporation of cyclic grafts into the star-shaped architecture provides yet another synthetic route to control structure and dynamics of polymers via topology. Hybrid star polymers (also called *rosette polymers*) consisting of f_L linear chains and f_R cyclic polymers fused at the central point are currently the subject of intensive experimental [47–51] and theoretical studies [51–55].

In the present work we investigate theoretically the basic conformational properties of rosette polymers in a good solvent. Our focus is on the degree of compactness of hybrid stars with increasing functionality of linear and cyclic arms. The quantitative description of the relative decrease in size is calculated through the size ratio [2]:

$$g = \frac{\langle R_g^2 \rangle_{\text{branched}}}{\langle R_g^2 \rangle_{\text{linear}}}. \quad (1)$$

The quantity g compares the size of a branched polymer to that of a linear one of the same total degree of polymerization. The ratio g is known to be universal in a sense that it does not depend on the microscopic details of the macromolecules but on the global parameters such as space dimension, solvent quality, or branching parameters. In this study we estimate g using an analytical theory based on the path-integration method as

*jaroslaw.paturej@us.edu.pl

well as extensive bead-spring coarse-grained molecular dynamics (MD) simulations.

The paper is organized as follows. In Sec. II we study the conformational properties of hybrid stars analytically by means of the continuous chain model. In Sec. III we describe the details of the used simulation methods. In the same section we present the obtained numerical results and compare them with our theoretical predictions. We conclude our findings in Sec. IV.

II. ANALYTICAL THEORY

A. Model

Our theoretical treatment of the conformational properties of rosette polymers in good solvents is based on the continuous chain model [56]. In this model, polymer chains are described as $3d$ trajectories, with radius vectors $\vec{r}_i(s)$ ($i = 1, \dots, f_L + f_R$), parametrized by s changing from 0 to L , where L is the total arc length of the trajectory. All $f_L + f_R$ trajectories start at the origin and f_R of them form closed loops. The partition function of this system is defined as [52]

$$Z^{f_L, f_R} = \frac{1}{Z_0} \prod_{i=1}^{f_L + f_R} \int d\vec{r}_i(s) \delta(\vec{r}_i(0)) \delta(\vec{r}_i(L) - \vec{r}_i(0)) e^{-H}, \quad (2)$$

where δ functions are used to impose constraints on the trajectories such that they start at the origin and form loops, respectively. Z_0 is the partition function of the Gaussian chain given by

$$Z_0 = \prod_{i=1}^{f_L + f_R} \int d\vec{r}_i(s) e^{-\sum_{i=1}^{f_L + f_R} \int_0^L ds \left(\frac{d\vec{r}_i(s)}{ds} \right)^2}. \quad (3)$$

In Eq. (2) H is the system Hamiltonian:

$$H = \sum_{i=1}^{f_L + f_R} \int_0^L ds \left(\frac{d\vec{r}_i(s)}{ds} \right)^2 + \frac{u}{2} \sum_{i,j=1}^{f_L + f_R} \int_0^L ds' \int_0^L ds'' \delta(\vec{r}_i(s') - \vec{r}_j(s'')), \quad (4)$$

where the first term describes polymer connectivity and the second term represents excluded volume interactions with the coupling constant, u .

It is important to note that cyclic polymers usually have more complicated topological constraints as compared to linear chains. In particular different types of knots can be present. The partition sum in our case is taken over all the possible configurations, including all possible knot types. We are considering a model in its asymptotic limit where monomers are considered as points on the infinitely long trajectory [57]. Under these conditions knots are localized and do not influence either scaling exponents or the critical amplitudes [58–60].

Within the frames of the continuous chain model the excluded volume effect is treated as perturbation of the Gaussian model and the perturbation theory in parameter u is applicable

in this case. To evaluate the quantitative estimates for universal observables of interest, the advanced renormalization schemes are applied, which are described below. The main general idea of these approaches is removal of divergencies which are encountered in the asymptotical limit $L \rightarrow \infty$. This can be achieved by a controlled rearrangement of the perturbation theory series.

B. Direct renormalization scheme

Within Cloiseaux's direct renormalization [57], a set of renormalization factors are introduced that are directly connected to the physical quantities and allow one to remove those divergencies. Within the continuous chain model, the Hamiltonian of the system does not contain any reference towards the particular topology that is considered. As a result, the fixed points of the scheme do not depend on the topology and can be calculated for the simplest case of a single linear chain and then used in the description of more complicated polymer architectures. For this scheme the renormalized coupling constant is introduced as

$$u_R(u_0) = -[Z(L, u_0)]^{-2} Z(L, L) [2\pi \chi_0(L, u_0)]^{-2+\epsilon/2}, \quad (5)$$

where $Z(L, L)$ is the partition function of two interacting polymers, $\epsilon = 4 - d$ stands for the deviation from the upper critical dimension, d denotes the spatial dimension, and the dimensionless coupling constant u_0 is defined by

$$u_0 = u(2\pi)^{-d/2} L^{2-d/2}. \quad (6)$$

The renormalization factors that are introduced in this expression are connected with the number of allowed trajectories or the partition function of a single chain, $[Z(L, u_0)]^{-2}$, and with its characteristic size, i.e., the end-to-end distance, $\langle R_e^2 \rangle$, or more precisely with the swelling factor, $\chi_0(L, \{x_0\})$, defined as $\chi_0 = \langle R_e^2 \rangle / L$. The introduction of these factors leads to the finite value of u_R in the limit of infinitely long chains, unlike u_0 that in the same limit is divergent:

$$\lim_{L \rightarrow \infty} u_R(u_0) = u_R^*. \quad (7)$$

In practical applications the value u_R^* can be calculated from the equation

$$\beta_{u_R} = 2L \frac{\partial u_R(u_0)}{\partial L} = 0. \quad (8)$$

For the simplest case of a Gaussian polymer (without excluded volume interactions) and a real polymer (with excluded volume interactions) the solutions for u_R^* are well known [57] and given by the following equations:

$$\text{Gaussian: } u_R^* = 0, \quad (9)$$

$$\text{EV: } u_R^* = \frac{\epsilon}{8}. \quad (10)$$

C. Douglas-Freed approximation for the universal size ratios

The renormalization group approach described above allows one to calculate observables that can be directly compared to experimental and simulation results only if the analytical calculations are made up to at least the second order terms in the coupling constant u_0 . Note that this is a

complicated task for nonlinear polymer architectures since the number of diagrams that have to be taken into account and their mathematical complexity increase tremendously. At this point it is useful to consider the connection between the continuous chain model and the two-parameter model in three spatial dimensions ($d = 3$). It enables us to use the approximation developed by Douglas and Freed [6] that allows better concurrence between the renormalization group in the first order and experimental data.

It is a well known fact that any observable calculated in the renormalization group approach can be presented in a form of a universal function [6,61]. Such a function for a radius of gyration, R_g , reads

$$\langle R_g^2 \rangle = \langle R_{g/0}^2 \rangle \left(\frac{2\pi N}{\Lambda} \right)^{2\nu(\eta)-1} f_p(\eta), \quad (11)$$

where N is the number of monomers, Λ is the coarse-graining length scale, and $f_p(\eta)$ is the function that controls the solvent quality with η being the crossover variable. For a Gaussian chain $\eta = 0$ and $f_p(\eta) = 1$. The case of a polymer in an athermal solvent is recovered in the limit $\eta \rightarrow \infty$ with $f_p(\eta) = 1 + a$, where a is the topology-dependent parameter.

Note that the form of Eq. (11) is the same for any polymer topology. Thus we can write the size ratio of two different architectures in the following form:

$$g_x = \frac{\langle R_{g,1}^2 \rangle_0}{\langle R_{g,2}^2 \rangle_0} \frac{1 + a_1}{1 + a_2}, \quad (12)$$

where x is the generic subscript which can refer either to linear chains ($x = c$) or to star polymers ($x = s$). In the case of a linear chain it is possible to get the parameters a_1 and a_2 from the renormalization group approach by conducting the calculations up to at least quadratic terms ϵ^2 [6]. However, apart from that simple topology such calculations proved to be complicated and it is more convenient to use the two-parameter model for which the radius of gyration is obtained at the first order in the perturbation parameter z from the following formula:

$$\langle R_g^2 \rangle = \langle R_{g/0}^2 \rangle (1 + Cz), \quad (13)$$

with z being the counterpart of u_0 in two-parameter models with fixed $d = 3$ space dimension. In the equation above C is the function of branching parameters calculated in a three dimensional space which is related to the parameter a via

$$a = \frac{3}{32}C - \frac{1}{4}. \quad (14)$$

D. Analytical results

a. The partition function. The starting point of our calculations is the partition function defined by Eq. (2). The perturbation expansion is performed over the excluded volume coupling constant, u , as required by the general scheme of calculations for this model [57,62]. The first order expansion reads

$$Z^{f_L, f_R} = \frac{1}{Z_0} \prod_{i=1}^{f_L + f_R} \prod_{j=1}^{f_R} \int d\vec{r}_i(s) \delta(\vec{r}_i(0)) \delta(\vec{r}_j(L) - \vec{r}_j(0)) e^{-H_0}$$

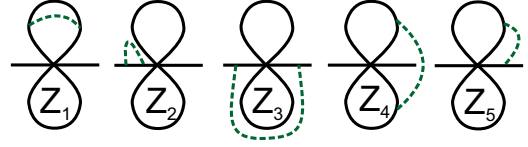


FIG. 1. Diagrammatic representation of contributions to the partition function of a rosette polymer in the one loop approximation. The solid lines denote polymer paths of length L and the dashed lines present the excluded volume interactions between points s' and s'' .

$$-\frac{u}{2} \frac{1}{Z_0} \prod_{i=1}^{f_L + f_R} \prod_{j=1}^{f_R} \int d\vec{r}_i(s) \delta(\vec{r}_i(0)) \delta(\vec{r}_j(L) - \vec{r}_j(0)) \times \sum_{i,j=1}^{f_L + f_R} \int_0^L ds' \int_0^L ds'' \delta(\vec{r}_i(s') - \vec{r}_j(s'')) e^{-H_0}, \quad (15)$$

with $H_0 = \sum_{i=1}^{f_L + f_R} \int_0^L ds \left(\frac{d\vec{r}_i(s)}{ds} \right)^2$ being the Hamiltonian of the Gaussian model. In order to calculate the first and Gaussian term in the partition function we use the integral representation of the $\delta(\vec{r}_j(L) - \vec{r}_j(0))$ functions that describe the looping of f_R chains. After performing all integrations we recover the known expression for rosette polymers [52]:

$$Z_0^{f_L, f_R} = (2\pi L)^{-\frac{d}{2} f_R}. \quad (16)$$

To calculate the contribution due to excluded volume interactions [given by the second term in expression (15)] we have used the diagrammatic technique as presented in Fig. 1. The analytical expressions corresponding to these diagrams as functions of the space dimension, d , read

$$\begin{aligned} Z_1 &= -2u_0 (2\pi L)^{-\frac{d}{2} f_R} \frac{\Gamma(2 - \frac{d}{2})^2}{(d-2)\Gamma(3-d)}, Z_2 \\ &= u_0 (2\pi L)^{-\frac{d}{2} f_R} \frac{4}{(4-d)(2-d)}, \\ Z_3 &= u_0 (2\pi L)^{-\frac{d}{2} f_R} \frac{4(2^{2-d/2} - 2)}{(4-d)(2-d)}, Z_4 \\ &= u_0 (2\pi L)^{-\frac{d}{2} f_R} \left(-\frac{1}{8} \frac{2^d \sqrt{\pi} \Gamma(1 - \frac{d}{2})}{\Gamma(\frac{5-d}{2})} \right. \\ &\quad \left. + \frac{1}{3} \frac{2^{d-1} 5^{-\frac{d}{2}} [{}_2F_1(\frac{3}{2}, \frac{d}{2}; \frac{5}{2}; \frac{1}{5}) - 3 {}_2F_1(\frac{1}{2}, \frac{d}{2}; \frac{3}{2}; \frac{1}{5})]}{d-2} \right), \\ Z_5 &= u_0 (2\pi L)^{-\frac{d}{2} f_R} \frac{2^{\frac{d-1}{2}} \sqrt{\pi} {}_2F_1(\frac{1}{2}, \frac{d-1}{2}; \frac{3}{2}; \frac{1}{2}) \Gamma(1 - \frac{d}{2})}{\Gamma(\frac{3-d}{2})}, \end{aligned} \quad (17)$$

where u_0 was defined in Eq. (6). Here, $\Gamma(x)$ is the gamma function and ${}_2F_1(a, b; c; z)$ is the hypergeometric function. Each type of diagram presented in Fig. 1 has to be taken with a prefactor. For the diagrams Z_1 and Z_2 the prefactor is equal to the number of rings, f_R , and linear chains, f_L , respectively. The diagrams Z_3 and Z_5 have to be accounted for each pair

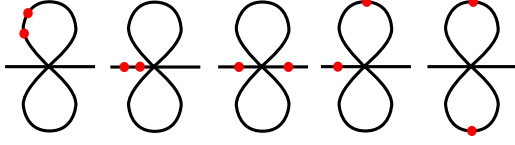


FIG. 2. Diagrammatic representation of contributions to the radius of gyration of rosette polymer in the Gaussian approximation. The solid lines represent polymer paths of length L . Bullets denote restriction points s_1 and s_2 .

of linear chains $[f_L(f_L - 1)/2]$ or rings $[f_R(f_R - 1)/2]$ and the diagram Z_4 for each pair of a single chain and a single ring $(f_L f_R)$. The ϵ expansion of the diagrams results in the partition function:

$$Z^{f_L, f_R} = (2\pi L)^{-\frac{d}{2} f_R} \left\{ 1 - u_0 \frac{f_L^2 + 4f_L f_R + 2f_R^2 - 3f_L + 2f_R}{\epsilon} - u_0 \left[\frac{f_L(f_L - 3)}{2} - \frac{f_L(f_L - 1)}{2} \ln(2) \right] + \frac{2}{5} f_L f_R \sqrt{5} \ln \left(\frac{2}{\sqrt{5} + 3} \right) + 2f_L f_R - f_R^2 - f_R - f_R(f_R - 1) \sqrt{2} \int_0^1 dt \frac{\ln(2-t)}{\sqrt{t(t-2)}\sqrt{4-2t}} \right\}. \quad (18)$$

Note that for $f_R = 1$ the above expression reproduces the result of our previous study [53].

b. The radius of gyration and the universal size ratios. Within the continuous chain model the radius of gyration of a rosette polymer is defined as

$$\langle R_g^2 \rangle = \frac{1}{2L^2(f_L + f_R)^2} \times \sum_{i,j=1}^{f_L + f_R} \int_0^L \int_0^L ds_1 ds_2 \overline{[\vec{r}_i(s_2) - \vec{r}_j(s_1)]^2}. \quad (19)$$

Here and below, $\langle \dots \rangle$ denotes averaging with the effective Hamiltonian Eq. (4) according to the recipe

$$\langle \dots \rangle = \frac{\prod_{i=1}^{f_L + f_R} \int d\vec{r}_i(s) \delta(\vec{r}_i(0)) \delta(\vec{r}_j(L) - \vec{r}_j(0)) e^{-H}}{Z^{f_L, f_R}}.$$

In order to calculate the average we use the identity

$$\overline{[\vec{r}_i(s_2) - \vec{r}_j(s_1)]^2} = -2 \frac{d}{d|\vec{k}|^2} \xi(\vec{k})_{\vec{k}=0}, \quad \xi(\vec{k}) \equiv \langle e^{-i\vec{k}[\vec{r}_i(s_2) - \vec{r}_j(s_1)]} \rangle, \quad (20)$$

and evaluate $\xi(\vec{k})$ in the path integration approach. In the calculation of the contributions to $\xi(\vec{k})$ it is again useful to use a diagrammatic presentation. The corresponding diagrams for a Gaussian polymer are displayed in Fig. 2. Taking into account that each diagram is taken with the appropriate prefactor, as it was in the case of partition functions in Eq. (17), we recover the known expression for the radius of gyration of a rosette

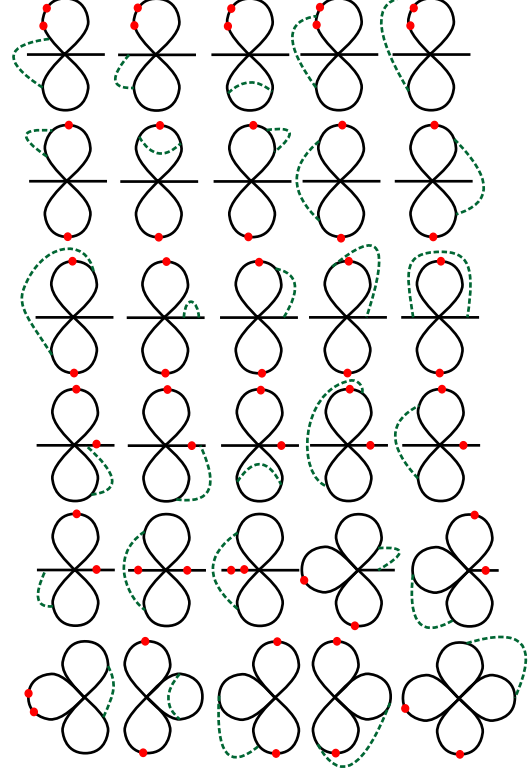


FIG. 3. Diagrammatic representation of the contributions to the radius of gyration of rosette polymer in a good solvent coming from the interactions that involve more than one ring. The solid lines represent polymer paths of length L . Bullets denote restriction points s_1 and s_2 , whereas dashed lines display the excluded volume interactions between points s' and s'' .

polymer in Gaussian approximation [52]:

$$\langle R_{g/0,r}^2 \rangle = \frac{2f_L(3f_L - 2) + 8f_L f_R + f_R(2f_R - 1)}{12(f_L + f_R)^2}. \quad (21)$$

Similarly, in the one loop approximation one has to calculate a set of diagrams that will contribute to $\xi(\vec{k})$, where each diagram contains both the restriction points, s_1 , s_2 , and the interaction points, s' , s'' . For a rosette polymer there is a set of 88 diagrams and 58 of them were calculated in our previous work [53]. The additional 30 diagrams which constitute the theoretical result of this work are presented in Fig. 3. These additional diagrams contribute to the interactions that involve more than one ring polymer. The general expression for the radius of gyration of a rosette polymer in a good solvent calculated in the one loop approximation as a series of ϵ reads

$$\langle R_g^2 \rangle_r = \langle R_{g/0,r}^2 \rangle \left(1 + \frac{2u_0}{\epsilon} - u_0 R_1(f_L, f_R) \right), \quad (22)$$

where $R_1(f_L, f_R)$ is the function of branching parameters f_L and f_R and is defined by Eq. (A1) in Appendix A.

To quantify the size properties of a rosette polymer in comparison with other molecular architectures we introduce two size ratios:

$$g_c = \frac{\langle R_{g/r}^2 \rangle}{\langle R_{g/c}^2 \rangle}, \quad (23)$$

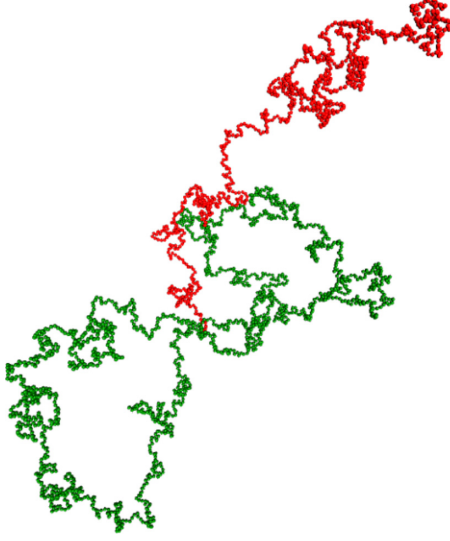


FIG. 4. Molecular dynamics simulation snapshot of a rosette polymer comprised of $f_R = 2$ ring arms and $f_L = 1$ linear arms. The degree of polymerization, N , of each arm is 1000. The linear arm is depicted in red and the ring arms are in green.

$$g_s = \frac{\langle R_{g,r}^2 \rangle}{\langle R_{g,s}^2 \rangle}, \quad (24)$$

$$(25)$$

where $\langle R_{g,c}^2 \rangle$ and $\langle R_{g,s}^2 \rangle$ are the radii of gyration of a linear chain and a star-shaped polymer comprised of linear polymers, respectively. Both ratios g_c and g_s are calculated for architectures with the same molecular weight as rosettes. The corresponding expressions for $\langle R_{g,c}^2 \rangle$ and $\langle R_{g,s}^2 \rangle$ are given by [62]

$$\langle R_{g,c}^2 \rangle = \frac{dL}{6[(f_L + f_R)L]} \left(1 + \frac{2u_0}{\epsilon} + u_0 \ln[(f_L + f_R)] - \frac{13}{12} \right), \quad (26)$$

$$\begin{aligned} \langle R_{g,s}^2 \rangle = & \frac{dL[3(f_L + f_R)^2 - 2f_L - 2f_R]}{6(f_L + f_R)^2} \left(1 + \frac{2u_0}{\epsilon} \right. \\ & + \frac{u_0}{12(3f_L + 3f_R - 2)} \{ 144(f_L + f_R)^2 \ln(2) \\ & + 195(f_L + f_R) - [384(f_L + f_R) \ln(2) \\ & \left. - 78(f_L + f_R)^2 + 240 \ln(2) - 130] \} \right). \quad (27) \end{aligned}$$

In the following section we compare our analytical findings with the results of simulations and experiments.

III. NUMERICAL SIMULATIONS

A. Simulation model

We consider a bead-spring, coarse-grained model [8] of a rosette polymer consisting of f_L linear and f_R ring arms tethered to a core monomer with a diameter σ . Each

arm is composed of N beads of the same size σ and equal mass connected by bonds. Thus the total number of monomers in the star (excluding the core) is $(f_L + f_R)N$. The bonds between subsequent beads are described by Kremer-Grest potential $V^{KG}(r) = V^{FENE}(r) + V^{WCA}(r)$ with the so-called finitely extensible nonlinear elastic (FENE) potential [63]:

$$V^{FENE}(r) = -0.5kr_0^2 \ln[1 - (r/r_0)^2]. \quad (28)$$

The nonbonded interactions between monomers are taken into account by means of the Weeks-Chandler-Anderson (WCA) interaction, i.e., the shifted and truncated repulsive branch of the Lennard-Jones potential given by

$$V^{WCA}(r) = 4\epsilon[(\sigma/r)^{12} - (\sigma/r)^6 + 1/4]\theta(2^{1/6}\sigma - r). \quad (29)$$

In Eqs. (28) and (29), r denotes the distance between the centers of two monomers (beads), while ϵ and σ are chosen as the units of energy and length, respectively. Accordingly, the remaining parameters are fixed at the values $k = 30\epsilon/\sigma^2$ and $r_0 = 1.5\sigma$. In Eq. (29) we have introduced the Heaviside step function $\theta(x) = 0$ or 1 for $x < 0$ or $x \geq 0$. In consequence, the steric interactions in our model correspond to good solvent conditions.

Newton's equations of motion were solved using the velocity-Verlet algorithm. The Langevin damping term with the coefficient $\zeta = 0.5m\tau^{-1}$ was added to maintain the temperature $T = \epsilon/k_B$, where k_B is the Boltzmann constant, $\tau = \sqrt{m\sigma^2/\epsilon}$ is the LJ unit time and m is the monomer mass. The integration step employed to solve the equations of motions was taken as $\Delta t = 0.003\tau$. All simulations were performed in a cubic box with periodic boundary conditions imposed in all spatial dimensions. All simulations were carried out using the Large-scale Atomic Molecular Massively Parallel Simulator (LAMMPS) [64] and the simulation snapshots were rendered using the Visual Molecular Dynamics (VMD) [65].

Initially, star-shaped polymers were grown using a self-avoiding random walk technique and placed randomly in the simulation cell. Simulations of rosette polymers were performed for the following number of monomer beads per arm: $N = 100, 500, 1000$, and 3000 . To improve the efficiency of conformational sampling each simulation was carried out with 12 identical molecules in the simulation box. The intermolecular interactions between the stars were turned off which corresponds to dilute solution conditions. In the first stage, simulations were carried out until the stars adopted their equilibrium conformations. This part of the simulation was running for at least three relaxation times, τ_R , defined as the relaxation time of the radius of gyration autocorrelation function. The required equilibration time depends on arms' functionality and their degree of polymerization. After equilibration we conducted production runs lasting up to $10^6 \tau$. The number of linear, f_L , and cyclic, f_R , arms of rosette polymers was varied between 1 and 4. The example conformation of a rosette polymer is displayed in Fig. 4. In the course of simulations the universal size ratios (23) and (24) were measured. Both ratios, g_c and g_s , are defined in the limit of infinitely long arms ($N \rightarrow \infty$). However, in numerical simulations we calculate these ratios for finite values

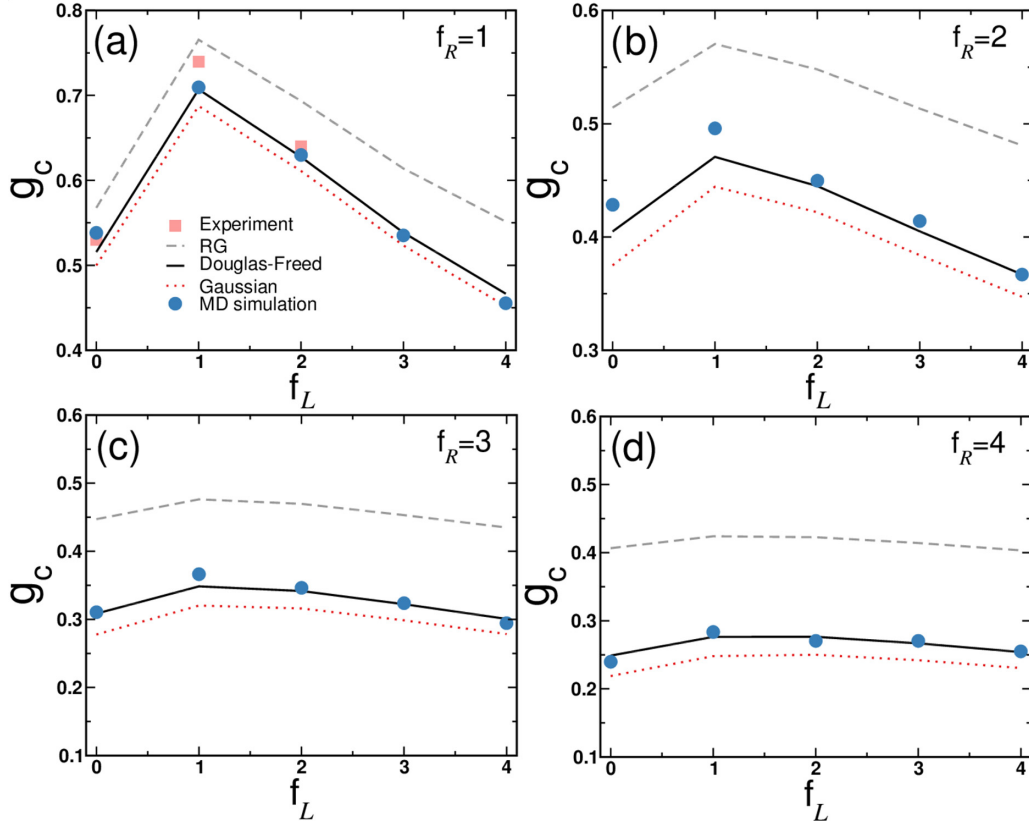


FIG. 5. Relative size ratio, g_c , of hybrid star polymers with respect to the size of linear polymers plotted as a function of the number of linear chains, f_L , for different number of grafted rings, f_R , as indicated. The lines represent theoretical predictions obtained for the Gaussian model (Ref. [52]) (dotted line), the renormalization group calculations (dashed line), and the Douglas-Freed approximation (solid line). The circles display results of molecular dynamics simulations. The experimental data for rings (Ref. [66]) ($f_R = 1$ and $f_L = 0$) and tadpoles (Ref. [48]) ($f_R = 1$ and $f_L = 1, 2$) are depicted by squares.

of N . In order to exclude finite-size effects from the calculated ratios we have used a least-square fitting of the form $g_i(N) = g_i + A_i/N$ for $i = c, s$ and with g_i and A_i being fitting constants.

B. Results and discussion

In Figs. 5–7 we display the overview of the theoretical and the numerical results as well as the available experimental data for the universal size ratios g_c and g_s of rosette polymers. The data in Figs. 5 and 7 are plotted as a function of the number of linear arms f_L for a fixed number f_R of grafted rings, whereas in Fig. 6 the data are displayed as a function of f_R for fixed values of f_L . As compared with the outcome of our simulations (circles) and the existing experiments [48,66] (squares), the analytical renormalization group calculations (dashed lines) reproduce only qualitatively the behavior of $g_c(f_L)$ and $g_s(f_L)$ profiles. In fact, the results of the renormalization group approach and the Gaussian approach [52] (dotted lines) serve, respectively, as the upper and the lower limit for the numerical and the experimental data. The Douglas-Freed approximation (solid lines), in turn, yields a significantly better agreement. This indicates that in order to get an improved quantitative concurrence with simulations higher order terms need to be included in the analytical approach. Due to complexity of the calculations

those terms were not taken into account in our renormalization group approach.

Note that the experimental values of the size ratios g_c^{expt} were obtained for polymers with relatively small molecular weights (up to $\approx 6 \times 10^4$ g/mol per polystyrene arm [48]). The entanglement molecular weight for polystyrene in a melt is $\approx 2 \times 10^4$ g/mol. It is known that entanglements of ring polymers are significantly suppressed as compared to linear counterparts [31]. Thus entanglement effects which affect conformations of star arms should not impact on g_c^{expt} in this case.

The numerically estimated relative size of a single ring polymer in a good solvent (i.e., for $f_R = 1, f_L = 0$) with respect to the size of a linear chain with the same N is $g_c^{\text{sim}} = 0.539$ [cf. Fig. 5(a)]. This value with a good accuracy reproduces our theoretical prediction which was calculated within the Douglas-Freed approximation, i.e., $g_c^{\text{DF}} = 0.516$. It is also very close to the experimentally measured relative size ratio $g_c^{\text{expt}} = 0.53$ [66]. The obtained ratios indicate the well-known feature of ring polymers, which adapt more compact conformations as compared to linear chains. Note that the values of $g_c^{\text{sim}}, g_c^{\text{DF}}$, and g_c^{expt} are slightly larger in comparison to the corresponding value of $g_c = 0.5$ known for ideal (Gaussian) rings [2]. For all considered rosette polymers (i.e., for $f_L > 0$) the size ratio, g_c , decays with increasing functionality of linear

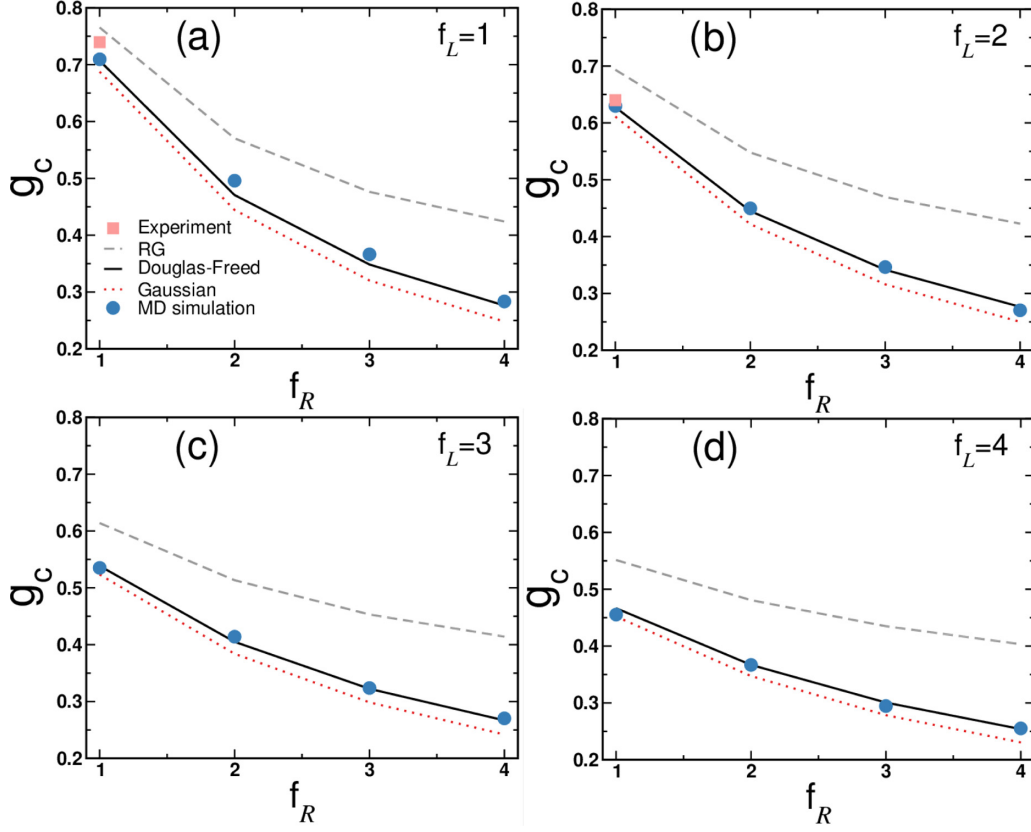


FIG. 6. Relative size ratio, g_c , of hybrid star polymers with respect to the size of linear polymers plotted as a function of the number of grafted rings, f_R , for different number of linear arms, f_L , as indicated. The convention of symbols and lines is the same as in Fig. 5.

arms (cf. Fig. 5). This trend is also in line with the available experimental data for tadpole conformations (i.e., for $f_R = 1$ and $f_L = 1$ or 2) [48]. A visual inspection of all panels in Fig. 5 indicates that the degree of compactness of rosette polymers with respect to linear polymers significantly increases with increasing the number of ring arms. The relative size ratio, g_s , of rosette polymers to stars comprised of solely linear arms is presented in Fig. 7. As expected, g_s for rosette polymers with the largest number of linear arms that was investigated in our study ($f_L = 4$) and with only one grafted ring ($f_R = 1$) tends to unity. Increasing the functionality of the grafted rings leads to systematic compactification of the rosettes with respect to star shaped polymers comprised of linear arms.

IV. CONCLUSIONS

In this work we have studied the conformational properties of rosette polymers with excluded volume using the analytical theory and simulations. We have determined the basic universal characteristics of these macromolecules in a good solvent by comparing their size to the size of linear chains of the same molecular weight (g_c ratio) and to the size of starlike polymers composed of the same number of solely linear arms (g_s ratio).

Our results indicate that conformations of rosette polymers are much more compact as compared to linear chains and corresponding star polymers. The degree of compactness of rosettes increases with increasing the functionality of grafted rings. The analytical calculations based on the Douglas-Freed approximation are in very good agreement with the estimates obtained from molecular dynamics simulations and experiments. Since the existing experimental data are limited we hope that our investigation will stimulate further experimental investigations on the behavior of complex polymer architectures in solutions.

ACKNOWLEDGMENTS

J.P. and K.H. would like to acknowledge the support from the National Science Center, Poland (Grant No. 2018/30/E/ST3/00428) and the computational time at PL-Grid, Poland.

APPENDIX

The prefactor $R_1(f_L, f_R)$ in Eq. (22) is defined by the following expression:

$$R_1(f_L, f_R) = -\frac{16800\pi f_R^2 - 109200f_L^3 - 189840f_L^2 f_R - 231167f_L f_R^2 - 16800\pi f_R + 273000f_L^2 + 333647f_L f_R}{8400(6f_L^2 + 8f_L f_R + 2f_R^2 - 4f_L - f_R)}$$

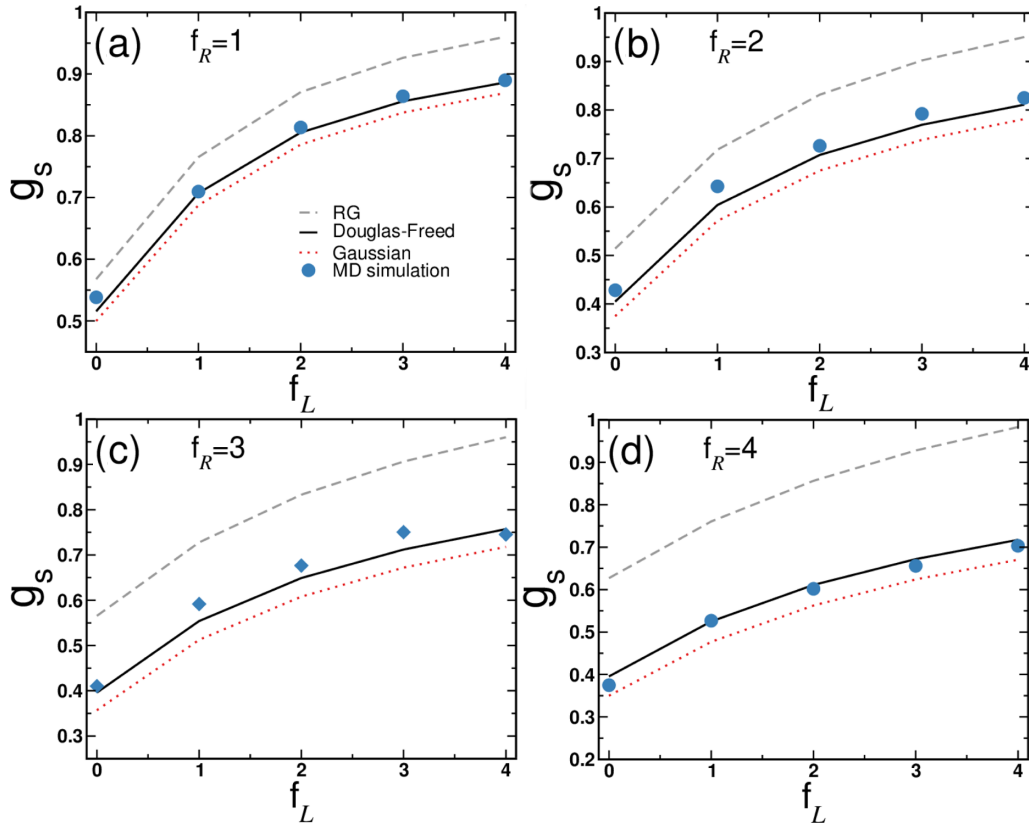


FIG. 7. Relative size ratio, g_s , of hybrid star polymers with respect to the size of star-shaped polymers with linear arms as a function of the number of linear chains, f_L , for different numbers of grafted rings, f_R , as indicated. The convention of symbols and lines is the same as in Fig. 5.

$$\begin{aligned}
 & + \frac{-50400f_R^2 - 182000f_L + 50400f_R}{8400(6f_L^2 + 8f_Lf_R + 2f_R^2 - 4f_L - f_R)} + \frac{2}{5}\sqrt{5}\ln(\sqrt{5} + 3)f_Lf_R - \frac{48f_Lf_R\ln(2)\sqrt{5}}{120} \\
 & - \frac{\sqrt{5}f_Lf_R\operatorname{arctanh}\left(\frac{\sqrt{5}}{5}\right)}{4200} - \frac{20160f_L^2 + 26880f_Lf_R + 6720f_R^2 + 61824f_L + 141275f_R - 148667}{6f_L^2 + 8f_Lf_R + 2f_R^2 - 4f_L - f_R} \\
 & - \frac{f_L\ln(2)}{120} \frac{2880f_L^2 + 2880f_Lf_R - 197f_R^2 - 7680f_L - 2683f_R + 4800}{6f_L^2 + 8f_Lf_R + 2f_R^2 - 4f_L - f_R} \\
 & + f_R(f_R - 1) \frac{12f_L + 12f_R - 18}{8(6f_L^2 + 8f_Lf_R + 2f_R^2 - 4f_L - f_R)} + \frac{2f_R(f_R - 1)}{6f_L^2 + 8f_Lf_R + 2f_R^2 - 4f_L - f_R} \\
 & \times \int_0^1 dt \frac{\ln(2-t)(t^2 - 3t + 1)}{\sqrt{t}(2-t)^{3/2}} - f_R(f_R - 1) \frac{\sqrt{2}\operatorname{arctanh}\left(\frac{\sqrt{2}}{2}\right)(34f_L + 34f_R - 59)}{8(6f_L^2 + 8f_Lf_R + 2f_R^2 - 4f_L - f_R)} \\
 & + 8f_R(f_R - 1) \int_0^1 dt \operatorname{arctan}((4t^2 - 4t - 1)^{-1/2}) \frac{(t-1)[12t^2(t-1)(f_1+f_2) - 30t^4 + 39t^3 + 5t^2 - 14t - 2]}{(4t^2 - 4t - 1)^{5/2}(6f_L^2 + 8f_Lf_R + 2f_R^2 - 4f_L - f_R)}.
 \end{aligned} \tag{A1}$$

[1] C. N. Likos, *Phys. Rep.* **348**, 267 (2001).

[2] H. Zimm and W. H. Stockmayer, *J. Chem. Phys.* **17**, 1301 (1949).

[3] W. H. Stockmayer and M. Fixman, *Ann. N.Y. Acad. Sci.* **57**, 334 (1953).

[4] M. Doud and J. P. Cotton, *J. Phys. (Paris)* **43**, 531 (1982).

[5] A. Miyake and K. F. Freed, *Macromolecules* **16**, 1228 (1983).

[6] J. Douglas and K. F. Freed, *Macromolecules* **17**, 2344 (1984).

[7] S. G. Whittington, J. E. G. Lipson, M. K. Wilkinson, and D. S. Gaunt, *Macromolecules* **19**, 1241 (1986).

- [8] G. S. Grest, K. Kremer, and T. A. Witten, *Macromolecules* **20**, 1376 (1987).
- [9] J. Batoulis and K. Kremer, *Macromolecules* **22**, 4277 (1989).
- [10] J. F. Douglas, J. Roovers, and K. F. Freed, *Macromolecules* **23**, 4168 (1990).
- [11] A. J. Archer, C. N. Likos, and R. Evans, *J. Phys.: Condens. Matter* **14**, 12031 (2002).
- [12] J. Roovers and P. M. Toporowski, *J. Appl. Polym. Sci.* **18**, 1685 (1974).
- [13] E. Glynos, B. Frieberg, and P. F. Green, *Phys. Rev. Lett.* **107**, 118303 (2011).
- [14] T. C. B. McLeish, *Europhys. Lett.* **6**, 511 (1988).
- [15] H. Watanabe, Y. Matsumiya, and T. Inoue, *Macromolecules* **35**, 2339 (2002).
- [16] L. J. Fetters, A. D. Kiss, D. S. Pearson, G. F. Quack, and F. J. Vitus, *Macromolecules* **26**, 647 (1993).
- [17] T. Pakuła, D. Vlassopoulos, G. Fytas, and J. Roovers, *Macromolecules* **31**, 8931 (1998).
- [18] *Condens. Matter Phys.* **5** (1) (2002), special issue on star polymers, edited by C. von Ferber and Yu. Holovatch.
- [19] T. E. Kiovsky, Star-shaped dispersant viscosity index improver, Houston, TX, 1978.
- [20] G. S. Grest, L. J. Fetters, J. S. Huang, and D. Richter, *Adv. Chem. Phys.* **94**, 67 (1996).
- [21] N. Hadjichristidis, M. Pitsikalis, and H. Iatrou, Polymers with Star-Related Structures: Synthesis, Properties, and Applications, in *Macromolecular Engineering* (Wiley-VCH Verlag GmbH & Co. KGaA, Weinheim, Germany, 2011).
- [22] N. Yamaguchi and K. Kiick, *Biomacromolecules* **6**, 1921 (2005).
- [23] D. P. Yang, M. Oo, G. R. Deen, Z. Li, and X. J. Loh, *Macromol. Rapid Commun.* **38**, 1700410 (2017).
- [24] D. Vlassopoulos, R. Pasquino, and F. Slijkers, Progress in the Rheology of Cyclic Polymers, in *Topological Polymer Chemistry*, edited by Y. Tezuka (World Scientific, Singapore, 2014).
- [25] J. Roovers, *Macromolecules* **21**, 1517 (1988).
- [26] B. A. Laurent and S. M. Grayson, *Chem. Soc. Rev.* **38**, 2202 (2009).
- [27] J. D. Halverson, W. B. Lee, G. S. Grest, A. Y. Grosberg, and K. Kremer, *J. Chem. Phys.* **134**, 204905 (2011).
- [28] Y. Tezuka, *Polym. J.* **44**, 1159 (2012).
- [29] Z. Jia and M. J. Monteiro, *J. Polym. Sci. A* **50**, 2085 (2012).
- [30] K. Zhang and G. N. Tew, *React. Funct. Polym.* **80**, 40 (2014).
- [31] M. Kapnistos, M. Lang, D. Vlassopoulos, W. Pyckhout-Hintzen, D. Richter, D. Cho, T. Chang, and M. Rubinstein, *Nat. Mater.* **7**, 997 (2008).
- [32] K. Zhang, M. Lackey, J. Cui, and G. N. Tew, *J. Am. Chem. Soc.* **133**, 4140 (2011).
- [33] A. Erbas and J. Paturej, *Soft Matter* **11**, 3139 (2015).
- [34] G. Morgese, L. Trachsel, M. Romio, M. Divandari, S. N. Ramakrishna, and E. M. Benetti, *Angew. Chem.* **55**, 15583 (2016).
- [35] W. Fiers and R. L. Sinsheimer, *J. Mol. Biol.* **5**, 424 (1962).
- [36] H.-X. Zhou, *J. Am. Chem. Soc.* **125**, 9280 (2003).
- [37] L. J. Perry and R. Wetzell, *Science* **226**, 555 (1984).
- [38] J. A. Wells and D. B. Powers, *J. Biol. Chem.* **261**, 6564 (1986).
- [39] C. N. Pace, G. R. Grimsley, J. A. Thomson, and B. J. Barnett, *J. Biol. Chem.* **263**, 11820 (1988).
- [40] A. D. Nagi and L. Regan, *Folding Des.* **2**, 67 (1997).
- [41] P. Fraser, *Curr. Opin. Genet. Dev.* **16**, 490 (2006).
- [42] M. Simonis, P. Klous, E. Splinter, Y. Moshkin, R. Willemssen, E. de Wit, B. van Steensel, and W. de Laat, *Nat. Genet.* **38**, 1348 (2006).
- [43] J. Dorier and A. Stasiak, *Nucl. Acids Res.* **37**, 6316 (2009).
- [44] R. Schlieff, *Science* **240**, 127 (1988).
- [45] K. Rippe, P. H. von Hippel, and J. Langowski, *Trends Biochem. Sci.* **20**, 500 (1995).
- [46] K. B. Towles, J. F. Beausang, H. G. Garcia, R. Phillips, and P. C. Nelson, *Phys. Biol.* **6**, 025001 (2009).
- [47] Z.-C. Yan, Md. D. Hossain, M. J. Monteiro, and D. Vlassopoulos, *Polymers* **10**, 973 (2018).
- [48] Y. Doi *et al.*, *Macromolecules* **46**, 1075 (2013).
- [49] Y. Doi, A. Takano, Y. Takahashi, and Y. Matsushita, *Macromolecules* **48**, 8667 (2015).
- [50] D. E. Lonsdale and M. J. Monteiro, *Chem. Commun.* **46**, 7945 (2010).
- [51] M. D. Hossain, J. C. Reid, D. Lu, Z. Jia, D. J. Searles, and M. J. Monteiro, *Biomacromolecules* **19**, 616 (2018).
- [52] V. Blavatska and R. Metzler, *J. Phys. A: Math. Theor.* **48**, 135001 (2015).
- [53] K. Haydukivska and V. Blavatska, *Phys. Rev. E* **97**, 032502 (2018).
- [54] K. Haydukivska, V. Blavatska, and J. Paturej, *Sci. Rep.* **10**, 14127 (2020).
- [55] A. Rosa, J. Smrek, M. S. Turner, and D. Michieletto, *ACS Macro Lett.* **9**, 743 (2020).
- [56] S. F. Edwards, *Proc. Phys. Soc. London* **85**, 613 (1965); **88**, 265 (1965).
- [57] J. des Cloizeaux and G. Jannink, *Polymers in Solution: Their Modelling and Structure* (Clarendon Press, Oxford, 1990).
- [58] M. L. Mansfield and J. F. Douglas, *J. Chem. Phys.* **133**, 044903 (2010).
- [59] Y. Kantor, *Pramana, J. Phys.* **64**, 1011 (2005).
- [60] E. Orlandini and S. G. Whittington, *Rev. Mod. Phys.* **79**, 611 (2007).
- [61] Y. Oono, in *Advances in Chemical Physics, Volume LXI*, edited by I. Prigogine and S. A. Rice (John Wiley and Sons, Inc., New York, 1985).
- [62] V. Blavatska, C. von Ferber, and Yu. Holovatch, *Condens. Matter Phys.* **15**, 33603 (2012).
- [63] G. S. Grest and K. Kremer, *Phys. Rev. A* **33**, 3628 (1986).
- [64] S. Plimpton, *J. Comput. Phys.* **117**, 1 (1995).
- [65] W. Humphrey, A. Dalke, and K. Schulten, *J. Mol. Graph.* **14**, 33 (1996).
- [66] J. Higgins, K. Dodgson, and J. A. Semlyen, *Polymer* **20**, 553 (1979).